Optical Beamforming System Based on Polarization Manipulation With Amplitude–Phase Coupling Suppression

Shangzhe Xu, Xiangchuan Wang, Yue Yang, Cong Ma, Xi Liu, Lihan Wang, Xin Jiang, Xingwei Ye, and Shilong Pan, *Fellow, IEEE*

***Abstract*— Traditional phased arrays based on phase shifters suffer severely from the beam-squint problem when operating at the wideband mode. Optical beamforming is one feasible solution for broadband beam steering, of which the performance, however, is affected by the amplitude–phase coupling. To solve this problem, we propose an optical beamforming system with amplitude–phase coupling suppression based on polarization manipulation. A polarization controller is used to control the transmission of carrier light along the fast or slow axis in the polarization-maintaining fiber. As there is a fixed transmission time difference between the two orthogonal modes, the phase adjustment can be achieved with low amplitude variation because of the low polarization-dependent loss. In addition, the intensity of the signal can be controlled using a polarizer with negligible phase variation, realizing amplitude control with low phase coupling. Experimental results show that the amplitude–phase coupling coefficient is about 5.8×10^{-3} ps/dB, while the phase–amplitude coupling is less than 7.5×10^{-3} dB/ps. The performance of the optical beamforming is analyzed by numerical simulation and proof-of-concept experiment, showing that the beam pointing deflection is less than 0.1°, while the main-lobe-to-sidelobe suppression ratio deteriorates less than 1 dB when the beam scans from 0° to 45°.**

***Index Terms*— Amplitude–phase coupling, beamforming, phased array antenna, polarization control, polarization-maintaining fibers (PMFs), true-time delay (TTD).**

I. Introduction

PHASED arrays traditionally use phase shifters to control the beam direction, which shows great advantages in terms of fast beam scanning and high reconfigurability [1], [2]. With the demand for target recognition, a large bandwidth is required for a phased array to achieve high resolution. However, as the bandwidth increases, the beam-squint problem would present [3], [4], [5], [6]. To address this issue, beamforming based on optical true-time delays (TTDs) is considered an effective solution [7], [8], [9], [10].

In general, the approaches to implementing the TTD can be divided into several categories: 1) different propagating lengths switched by optical switches [11], [12], [13]; 2) fiber grating-based TTD [14], [15], [16]; and 3) optical dispersion with different input wavelengths [17], [18], [19]. The schemes mentioned above are applicable for broadband scenarios and provide a solid basis for microwave photonic phased array systems. However, the fiber grating-based TTD would easily cause amplitude–phase coupling due to the nonuniformity frequency response of fiber gratings [20]. Besides, for the dispersion-based TTD, the magnitude controlling is usually achieved using optical amplifiers and attenuators [21], [22], [23], [24], which will inevitably introduce a delay variation. The errors induced by the amplitude–phase coupling would significantly affect the performance of phased array systems, such as the power reduction of the main lobe, broadening of the main lobe, and raising of the sidelobe [25], [26]. One TTD without amplitude–phase coupling is achieved by utilizing two spatial light modulators (SLMs) to modify the amplitude and phase of the signal [27]. However, the insertion loss could be large because of the inefficient coupling between the free-space devices and the optical fiber. Besides, with the tremble of the free-space system, the optical power and path length of the spatial light injected into the optical fiber will be fluctuated. Therefore, new technologies with amplitude–phase coupling suppression for the optical beamforming system are highly anticipated.

In this article, we propose an optical beamforming network (OBFN) with large suppression of the amplitude–phase coupling based on optical polarization manipulation. A phase control module (PCM) is used to realize the TTD, which is implemented by regulating the polarization direction of a linearly polarized light along the fast or slow axis of a length of polarization-maintaining fiber (PMF) via a polarization controller (PC). The amplitude control is achieved by an amplitude control module (ACM) using a polarizer. With the suppressed amplitude–phase coupling, the OBFN performance, such as the accuracy of the beam direction and the main-lobe-to-sidelobe suppression ratio, is improved. This article is organized as follows. Section II describes the principle and composition of the OBFN. In Section III, the performance of the proposed amplitude and PCMs is analyzed

Manuscript received 17 April 2022; revised 4 November 2022; accepted 25 November 2022. This work was supported in part by the National Natural Science Foundation of China under Grant 62075095, in part by the Young Elite Scientists Sponsorship Program by China Association for Science and Technology (CAST) under Grant 2018QNRC001, in part by the Fundamental Research Funds for the Central University, and in part by the Key Research and Development Program of Jiangsu Province under Grant BE2020030. *(Corresponding authors: Xiangchuan Wang; Shilong Pan.)*

The authors are with the Key Laboratory of Radar Imaging and Microwave Photonics, Ministry of Education, Nanjing University of Aeronautics and Astronautics, Nanjing 210016, China (e-mail: wangxch@nuaa.edu.cn; pans@nuaa.edu.cn).

Color versions of one or more figures in this article are available at https://doi.org/10.1109/TMTT.2022.3226483.

Digital Object Identifier 10.1109/TMTT.2022.3226483

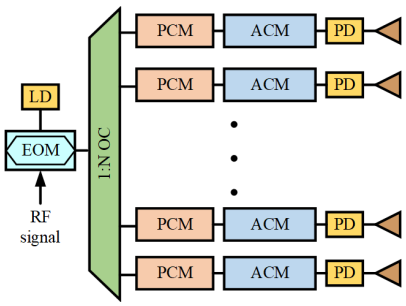

Fig. 1. Schematic of the proposed OBFNs. LD: laser diode. EOM: electrooptic modulator. OC: optical coupler. PCM: phase control module. ACM: amplitude control module. PD: photodetector.

in detail. In addition, the key performance of the OBFN link is investigated by numerical simulation. Finally, some concluding remarks are given in Section IV.

II. Principle

The schematic of the proposed system is shown in Fig. 1. The optical carrier is modulated by an RF signal in an electrooptic modulator (EOM). After distributing equally to N links by the coupler, signals are adjusted by the PCM and ACM based on polarization manipulation. Finally, the RF signals are emitted into space after square-law detection in the photodetector (PD). Here, we take a link to illustrate the principle in detail.

PMFs have two orthogonal polarization modes, fast and slow, with different refractive indexes, n_f and n_s, respectively. When a linearly polarized light travels through the fast and slow axes, there is a transmission time difference $\Delta\tau$, which depends on the length of the fiber, L, and beat length of the PMF, $l_p = \lambda/\Delta n$ ($\Delta n = n_f - n_s$). The time delay can be described as

$$\Delta\tau = \frac{L}{c/n_f} - \frac{L}{c/n_s} = \frac{L(n_f - n_s)}{c} = \frac{L/\lambda_c}{cl_p} \tag{1}$$

where c is the velocity of light in free space and λ_0 is the wavelength of the optic carrier produced by a laser diode (LD). If the light does not transmit along with the desired mode [28], [29], the phase of the photocurrent, I_c, will be

$$\varphi = \tan^{-1}\left[\frac{\sin^2\theta\sin(\omega\Delta\tau)}{\cos^2\theta - \sin^2\theta\cos(\omega\Delta\tau)}\right] \tag{2}$$

where θ is the angle between the fast axis and linearly polarized light and $\Delta\tau$ is the time difference of the light propagation along with the two modes of the PMF. When $\theta = 0$ or $\pi/2$, the module can be regarded as a TTD module, while the induced phase difference is $\omega\Delta\tau$.

Fig. 2 shows the structure of the PCM based on polarization, composed of N minimum delay units shown in the dotted box. The delay control unit includes a polarization switch and a PMF. A series of delay control units realize $\Delta\tau$, $2\Delta\tau$, $4\Delta\tau$, ..., $2^{n-1}\Delta\tau$ delay differences, which constitutes an N-bits step delayer. Since the loss difference between the two orthogonal polarization modes is small [30], the signal amplitude fluctuation error could be ignored.

The structure of the optical ACM is shown in Fig. 3, including a PC and polarizer. In the diagram, the blue dashed line indicates the orthogonal polarization coordinate system

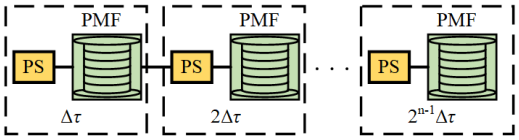

Fig. 2. Structure of PCM. The minimum delay control unit is in the dotted box. The PCM consists of N delay units. PS: polarization switch. PMF: polarization-maintaining fiber.

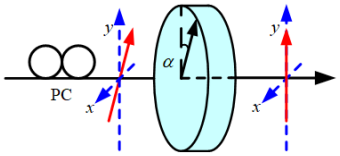

Fig. 3. Structure of PCM. The cylinder represents the polarizer, and α is the angle between the polarization direction of the light and the polarizer's transmission axis. PC: polarization controller.

with the polarization directions x and y. When the linearly polarized light passes through the polarizer, the output light field is the projection of the original light field on the polarizer transmission axis. By tuning the PC, the magnitude of the output light field can be adjusted to achieve the output signal amplitude control. Assuming that a linearly polarized light with single-sideband modulation is injected into the ACM, the expression can be described as

$$E \propto J_0(\gamma) + jJ_1(\gamma)e^{j\omega_m t} \tag{3}$$

where γ is the modulation index, J_n is the nth-order Bessel function of the first kind, and ω_m is the angular frequency of the RF signal. Then, the output signal of the polarizer is $E_{\text{out}} = E\cos\alpha$, where α is the angle between the input polarization direction and the polarizer transmission axis. After square-law detection, the electric field can be written as

$$I(t) \propto \cos^2\alpha\left[J_0^2(\gamma) + J_1^2(\gamma)\right] - 2\cos^2\alpha J_0(\gamma)J_1(\gamma)\sin(\omega_m t). \tag{4}$$

Ignoring the dc component, the excitation signal transmitted to the antenna is $2\cos^2\alpha J_0(\gamma)J_1(\gamma)\sin(\omega_m t)$. It can be seen from (4) that the amplitude of the excitation signal is only determined by the angle of polarization angle without inducing the phase coupling. Since the delay introduced by the polarizer is on the order of femtoseconds, the phase change of the RF signal can be disregarded, thus achieving amplitude control with low phase-to-amplitude coupling.

III. Experiment and Simulation Results

The performance of the PCM and ACM is experimentally tested. In addition, the performance of the OBFN network shown in Fig. 1 is also analyzed with numerical simulation.

A. Performance of PCM

In the experiment, 12 PMFs with lengths from 10 to 65 m are tested. The delay difference between two orthogonal polarizations of PMFs is measured using a self-developed high-precision optical delay meter with a delay precision of up to ±0.1 ps [31]. The fitting curve of delay difference and length is shown in Fig. 4. The red line is the fitting curve with a slope of 1.28 ps/m. The length error of the fiber has a

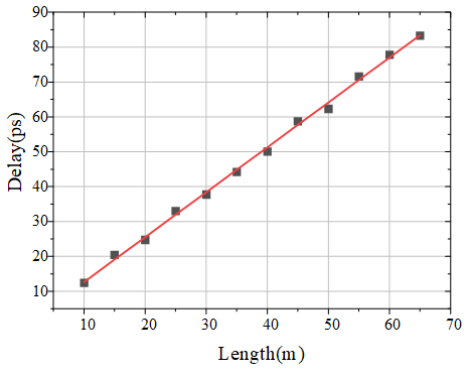

Fig. 4. Delay difference of two polarization modes of PMFs and fitting curve. The black points are test points. The red line is the fitting curve with a slope of 1.28 ps/m of the test results.

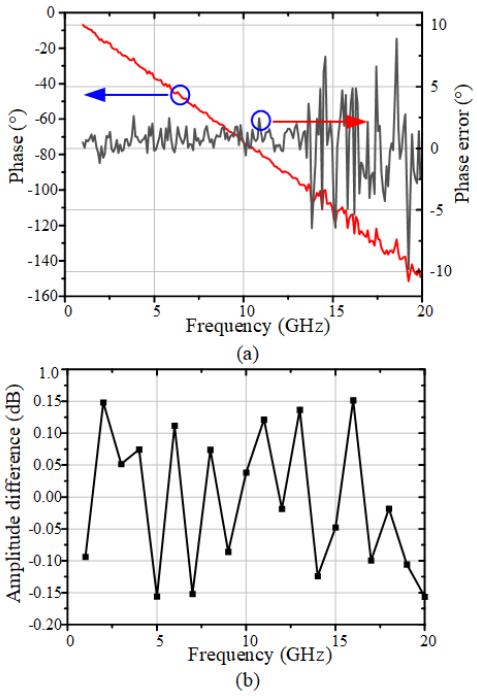

Fig. 5. Experimental results of PCM. (a) Phase difference (red line) between fast and slow modes of 15-m PMF. The phase error (black line) between the measured phase and the reference phase. (b) Amplitude difference.

much lower impact on the required delay difference compared with single-mode fiber (SMF). For example, 1-ps delay can be achieved using 0.78-m PMF, while it should be obtained by 0.2-mm SMF in traditional TTD, which is difficult to achieve such high accuracy length controlling in practice.

To investigate the RF phase controlling ability of the PCM, a measurement of the delay control unit is performed. A frequency sweep signal from 0 to 20 GHz with a power of 0 dBm is generated as the input RF signal by a vector network analyzer (VNA, Agilent NA-L N5235A). The optical carrier at 1550 nm with a power of 14.6 dBm produced by a narrow linewidth laser is modulated by the RF signal in a Mach–Zehnder modulator (MZM). After passing through the PCM, the optical signals are converted into electrical signals by PD. Finally, VNA receives the signal output from the unit.

The phase difference and amplitude difference of the signal transmitted along 15-m PMF are measured. Fig. 5(a) shows the phase error (black line), which is defined as the difference

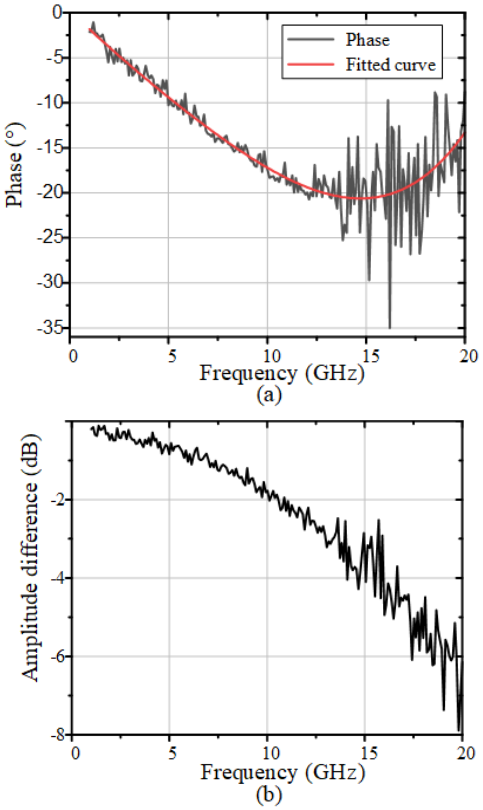

Fig. 6. Experimental results when light is not transmitted along with the fast or slow modes of PMF. (a) Phase difference. (b) Amplitude difference. PMF is 15 m long.

between the measured phase and the reference phase. It can be seen that the phase difference [red line of Fig. 5(a)] is linear to the frequency. The slope is about −7.4°/GHz (i.e., −20.61 ps at 10 GHz). In addition, the phase error is less than 2° (approximately 0.5 ps at 10 GHz). It should be noted here, as VNA can only produce about 13-GHz baseband signal, the higher frequency part is generated by frequency doubling with lower signal-to-noise ratio (SNR). A phase noise analyzer (ROHDE & SCHWARZ, Phase Noise Analyzer FSWP 1 MHz–50 GHz) is used to measure the amplitude of the signal in two orthogonal polarization modes separately. The amplitude difference of the output signal is plotted in Fig. 5(b). As can be seen, the amplitude difference of the signal is mainly concentrated in the ±0.2-dB range.

The necessity of an optical signal being injected along the fast or slow axis is also verified. When the light is not transmitted along with the fast or slow modes of PMF, the phase and amplitude controlling results are shown in Fig. 6. Fig. 6(a) shows the phase difference, showing nonlinearly with the frequency (red line, fit curve). It means that the PCM is not a TTD unit, which is not suitable for broadband beamforming. In addition, when controlling the phase through PCM, the amplitude of the RF signal varies with frequency as shown in Fig. 6(b), inducing large phase–amplitude coupling.

B. Performance of ACM

To analyze the performance of the ACM, the PC is rotated from 0° to 180°. A VNA is used to generate the 4–18-GHz sweep signal and monitor the amplitude change of the signals.

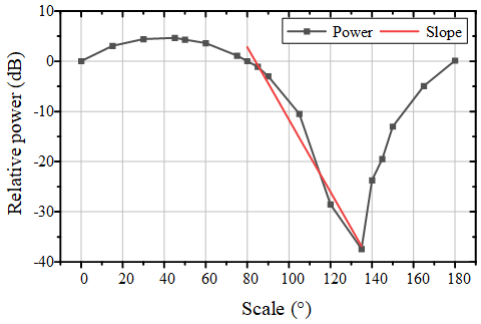

Fig. 7. Relationship between optical power and the scale of the PC. The black solid line with square markings is the power curve of the output signal from ACM. The red line is the slope of the first falling edge, −0.7215 dB/°.

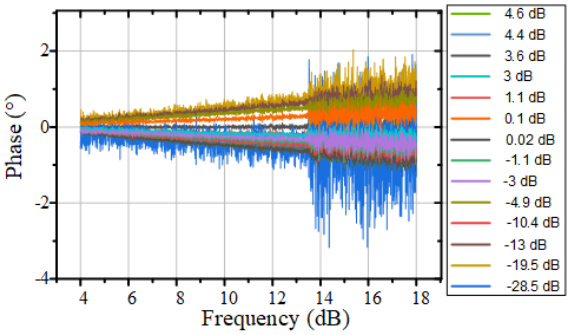

Fig. 8. Phase difference between received signals and reference.

The amplitude of the signal is used as the reference when the PC is set at the 0 scales. Fig. 7 shows the measured power of the output signal. The black solid line square markings are the power curve of the ACM output signal agreeing with the theory. To achieve amplitude controller, one edge range can be used, i.e., the first falling edge. The red line is the slope of the first falling edge, approximating −0.7215 dB/°. In addition, the amplitude adjustment range is about 42 dB.

The phase response of the ACM is further investigated. VNA is used to generate the 4–18-GHz sweep signal and acts as a phase discriminator to monitor the phase change of the signals. Rotating the polarizer at 0 scales, the output signal of ACM is taken as the reference. The phase variety introduced by the ACM is less than 2° (0.28 ps at 10 GHz) when the amplitude is adjusted within 33 dB, as shown in Fig. 8. Thus, the amplitude-to-phase coupling coefficient and the maximum coupling delay being obtained are 5.8×10^{-3} ps/dB and 0.28 ps, respectively. The ACM still introduces a delay, which may be caused by the fact that there is still a small angle between the input polarization of the light and the transmission axis of the polarizer. In addition, as the attenuation increases, the SNR deteriorates, inducing a larger phase difference jitter. The effective amplitude controlling range is about 33 dB.

C. Simulation of OBFN Based on Polarization Manipulation

In this section, we analyze the effect of the amplitude-to-phase and phase-to-amplitude coupling of PCM and ACM on the OBFN system. To evaluate the performance of the wideband OBFN, a correlation-maximum pattern (CMP) [32] is used. In addition, three key parameters (KPs), i.e., the value of the target direction (KP_1, relative value), the peak sidelobe level (PSLL, KP_2, relative value), and the average angle deviation to the target direction (KP_3), are extracted from the CMP to quantitatively analyze the impact of the amplitude–phase coupling.

TABLE I
PARAMETERS OF THE POLARIZATION-BASED OBFN IN CALCULATION

Parameter	Value
RF center frequency	10 GHz
Instantaneous bandwidth	4 GHz
Applied waveform	Linear frequency modulated
Number of antennas in the array	16
Antenna spacing	1.25 cm
Number of Polarization switches and PMFs in each channel	9

Based on the experimental results of ACM and PCM, the OBFN performance based on the proposed polarization controlling is simulated and analyzed. The common parameters are listed in Table I. Linear frequency modulation (LFM) signal with a time width of 0.1 ms and a bandwidth of 8–12 GHz is used as the RF signal. The PCM is set up as a 9-bit step delayer with a step of 1 ps. To avoid the effect of the grating lobe, the spacing between two adjacent elements is 1.25 cm, which is half of the minimum RF wavelength. Assume that the performance of each polarization switch of PCM is completely consistent. Similarly, the performance of the ACM of each link is consistent.

To study the effect of amplitude-to-phase coupling (caused by ACM) on the OBFN, we substitute the delay fluctuation as an influencing factor in the system. In the simulation, PCMs are adjusted to orient the main lobe of the OBFN to the direction of 30°, while the amplitude of the output signal of each link remains the same. The CMPs in three cases are compared. In the first case, i.e., the proposed scheme, we add to each link a random delay from 0 to 0.3 ps induced by amplitude-to-phase coupling of the ACM. In the second case, a random delay from 0 to 3 ps (±10.8° at 10 GHz) is added to each link to simulate the traditional ACM with large amplitude-to-phase coupling. In the last case, we obtain the CMP without amplitude-to-phase coupling as the reference.

The normalized CMPs of three cases are shown in Fig. 9, where the red line represents the results of the proposed scheme (the first case). The blue dotted line and the black dashed line depict the CMPs of the second and last cases, respectively. In addition, we tested the first two cases by ten times to obtain the average of their KPs. As can be seen, both CMPs of the proposed scheme and the case without coupling almost completely overlap. Compared to the ideal case, the main lobe of the second case deviated by 0.07°, while the PSLL increased by 0.17 dB. More power leaks from the main lobe (reduced by 0.015 dB) to the rest sidelobe, which results in an overall rise in the sidelobe.

To further analyze the effect of amplitude-to-phase coupling on OBFN, an experiment with different delay fluctuations is carried out. The fluctuation value is set to a random delay with a mean of 0 and a variance of x picoseconds, where x is an integer from 0 to 6. The main lobe is oriented in the direction of 30°. Fig. 10(a) shows the KP_1 (the value of the target direction on CMP), which decreases by 0.2 dB

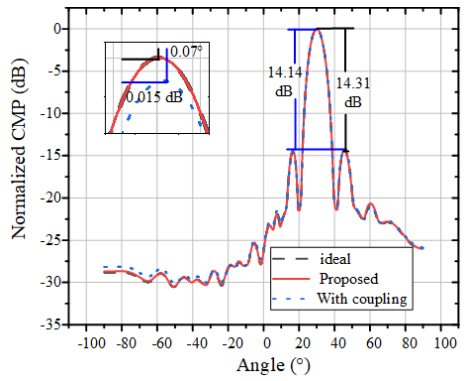

Fig. 9. CMPs of three different cases. The proposed scheme (red line, the random delay fluctuation from 0 to 0.3 ps). The case with coupling has the random delay fluctuation from 0 to 3 ps (blue dotted line). The case without coupling (black dashed line).

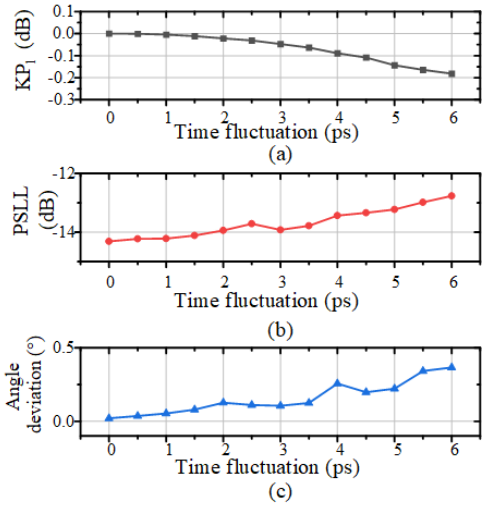

Fig. 10. Effect of amplitude-to-phase coupling on OBFN. (a) KP_1 (the value of the target direction on CMP). (b) PSLL. (c) Angle deviation to the target direction. The horizontal coordinate in the graph is the variance of the delay fluctuation.

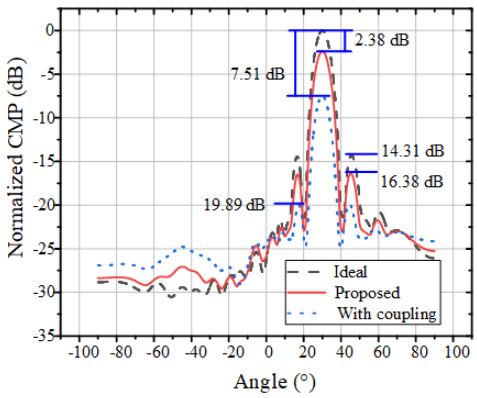

Fig. 11. CMPs of three different cases with different phase-to-amplitude coupling. First case: proposed scheme in which the loss between two work states of PCM is 0.3 dB, red line. Second case: loss between two work states of PCM is set as 1 dB, blue dotted line. Last case: without coupling, black dashed line.

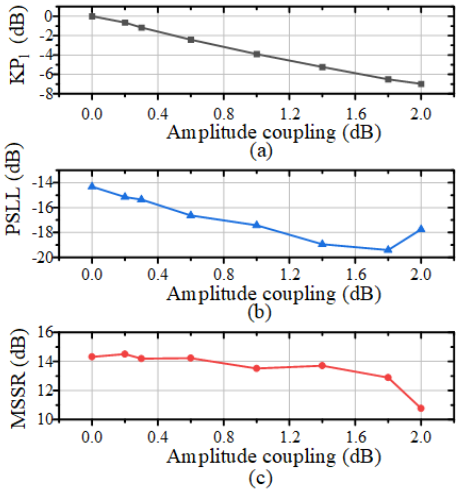

Fig. 12. Effect of phase-to-amplitude coupling on OBFN. (a) KP_1. (b) PSLL. (c) MSSR. The horizontal coordinate is the boundary value of the amplitude fluctuation interval.

as the phase variance increases. Fig. 10(b) shows that the effect of sidelobe suppression progressively deteriorates by about 1.57 dB. Besides, the angle deviation becomes larger with the maximum deviation angle of about 0.36°, as shown in Fig. 10(c). In total, the amplitude-to-phase coupling will shorten the irradiation distance and deflect the direction of OBFN, while the other sidelobes are raised.

The effect of phase-to-amplitude coupling (induced by PCM) on the performance of the OBFN system is also investigated. It is known from [30] that the polarization-dependent loss is less than 0.28 dB for all the differential group delays. Meanwhile, refer to the experimental results in Section III-B to set the simulation parameters. In the simulation, CMPs of three different cases are analyzed. In the first case, the amplitude coupling parameter is set as 0.3 dB. The parameter used in the second case is 1 dB to simulate the traditional PCM with large phase-to-amplitude coupling. The last case is the ideal case without coupling as a reference. The orientation of the main lobe is still set to 30°. The CMPs are given in Fig. 11. showing that the main lobe decreases in the first two cases (2.38 and 7.51 dB) compared to the ideal one. The proposed PCM achieves suppression of the sidelobe for about 5.1 dB.

To further investigate the effect of phase-to-amplitude coupling on CMPs, we set the amplitude difference between two work states of PCMs to different values. Considering that the amplitude difference is fluctuating, the phase-to-amplitude coupling term of each link is a random variable selected in $[0, x]$. The number x takes the values from 0 to 2 dB, while the main lobe is steered to 30°. The average results of multiple tests are shown in Fig. 12, in which Fig. 12(a) and (b) shows the KP_1 and the PSLL, respectively. Fig. 12(c) represents the main-lobe-to-sidelobe suppression ratio (MSSR) under different phase-to-amplitude coupling. It can be seen that as the phase-to-amplitude coupling becomes larger, the value of KP_1 steadily drops by about 7 dB, while PSLL decreases. In addition, the worst MSSR is reduced by about 3.7 dB.

In actual application, the coupling would exist in both the PCM and the ACM. Therefore, the simulation results are also given with amplitude-to-phase and phase-to-amplitude coupling simultaneously. The coupling term is set as mentioned before. By adjusting the PCM and ACM, the beam is steered to 30°, while the output signal amplitude is the same for each link. In the first one, two parameters of coupling are set as x (a random number selected in (0, 0.3) ps) and y (a random

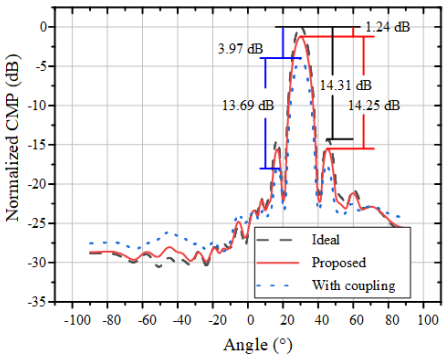

Fig. 13. Three CMPs. The first one is the proposed scheme (red line) with (0, 0.3) ps time fluctuation and (0, 0.3) dB amplitude coupling. The second one is the control group with amplitude and phase coupling (blue dotted line) with (0, 3) ps time fluctuation and (0, 1) dB amplitude coupling. The last one is the case without coupling (black dashed line).

number selected in (0, 0.3) dB), while x and y in the second case are selected in (0, 3) ps and (0, 1) dB, respectively. The last case without coupling is treated as a reference. The CMPs are given in Fig. 13. Compared to the proposed scheme, KP_1 of the second case is attenuated by 2.73 dB, while the MSSR increases by 0.56 dB from 14.25 dB.

Since the working state of the delay units in the PCM is determined by the direction of the main lobe, the performance of the OBFN at different orientations is also investigated. The main lobe of the OBFN is scanned from 0° to 45°. Simulation analyses of two cases are carried out, where the first case is the proposed scheme, while the second one is the case with coupling. The performance of the proposed OBFN is characterized by the average results of multiple tests, which are shown in Fig. 14. As can be seen, the KP_1s of case one in Fig. 14(a) decrease with the increase of the azimuth angle, while the change is less than 1.5 dB. Fig. 14(b) shows the sidelobe suppression effect of the OBFN in different orientations. Compared with the second case, the MSSR of the proposed scheme deteriorates within 1 dB. Moreover, the directivity of the proposed case [see Fig.14(c)] has a maximum angle deflection of less than 0.02°.

D. Experimental Verification of OBFN Based on Polarization Manipulation

According to the theory of generalized pattern multiplication [33], the field radiated by a phased array system can be obtained by multiplying the spectrum of the reference wave, the response of the single antenna, and the frequency-dependent array factor. The CMP of the OBFN system can be obtained by correlating the radiation field function with the reference waveform in the time domain. Because the spectrum of the reference wave and the response of the single antenna are usually known functions, we simply need to measure the array factor to calculate the radiation field. To obtain the array factor, the response of each channel in OBFN is measured with the experimental setup, as shown in Fig. 15(a). An optical carrier is modulated via MZM with 8–12-GHz frequency swept signals generated by the VNA. After passing through the PCM and ACM, the optical signal is converted into an electrical signal through PD and received by

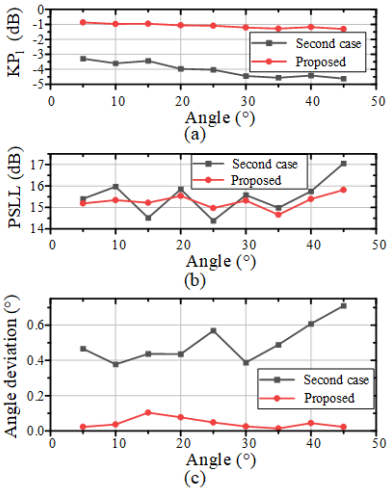

Fig. 14. OBFN performance of two cases. The first one is the proposed scheme (red line with circle markers). The second one is the case where both amplitude and phase coupling exist (black dashed line with triangle markers). (a) KP_1. (b) PSLL (KP_2). (c) Angle deviation.

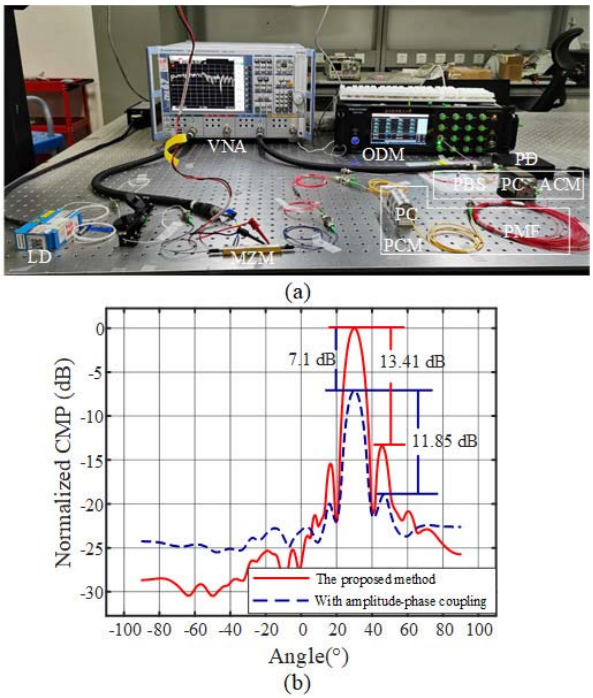

Fig. 15. (a) Photograph of the experimental setup for measuring the transmission response of the photonic link. (b) Two CMPs. The first one is the proposed scheme (red line) based on the experiment. The second one (blue line) is the results with amplitude–phase coupling.

the VNA. In addition, an optical delay meter is used to monitor the transmission delay of the light in the PMF. To simplify the description, light transmitted along the fast axis of the PMF is described as state 0; otherwise, it would be in state 1. The responses of the 15-m PMF in states 0 and 1 are measured, where the measured delay difference between the two working states is 20.9 ps.

The delay difference between adjacent channels is set as 20.9 ps, while the total delay of each channel is consistent with the numerical simulation. Based on the experimental data, the

array factor of an OBFN with 16 channels can be obtained. Moreover, the reference waveform is given as a chirp signal of 8–12 GHz with a duration of 100 ns. Fig. 15(b) shows the normalized CMP (red line). As can be seen, the MSSR is 13.41 dB, while the 3-dB width of the main lobe is about 8.8°. As a comparison, a random delay error of (0, 3) ps and a random amplitude error of (0, 0.5) dB are added to each link. The average CMP (blue dashed line) is shown in Fig. 15(b). Compared with the system with amplitude and phase coupling, the main lobe amplitude and MSSR of the proposed method are improved by 7.1 and 1.56 dB, respectively.

IV. Conclusion

In conclusion, we proposed and experimentally proved a broadband OBFN based on polarization manipulation with amplitude–phase coupling suppression. With high birefringent properties of the PMF, high-precision delay and amplitude controlling with a low amplitude–phase coupling are achieved. The experimental results show that the amplitude-to-phase coupling induced by ACM is approximately 5.8×10^{-3} ps/dB, while the phase-to-amplitude coupling induced by PCM is less than 7.5×10^{-3} dB/ps. In the numerical simulation, the beam pointing of the proposed OBFN system deflected less than 0.1°, while the MSSR deteriorates less than 1 dB when the beam scans from 0° to 45°.

References

[1] A. Y. Harper, "Introduction to phased array radars," in *Proc. SPIE, Effective Utilization Opt. Radar Syst.*, vol. 128, Dec. 1977, pp. 98–102.

[2] D. Parker and D. Z. Zimmermann, "Phased arrays—Part 1: Theory and architectures," *IEEE Trans. Microw. Theory Techn.*, vol. 50, no. 3, pp. 678–687, Mar. 2002.

[3] H. How et al., "Steerable phased array antennas using single-crystal YIG phase shifters-theory and experiments," *IEEE Trans. Microw. Theory Techn.*, vol. 48, no. 9, pp. 1544–1549, Sep. 2002.

[4] F. Akbar and A. Mortazawi, "Scalable phased array architectures with a reduced number of tunable phase shifters," *IEEE Trans. Microw. Theory Techn.*, vol. 65, no. 9, pp. 3428–3434, Sep. 2017.

[5] X. Ye, F. Zhang, and S. Pan, "Optical true time delay unit for multi-beamforming," *Opt. Exp.*, vol. 23, no. 8, pp. 10002–10008, Apr. 2015.

[6] T.-S. Chu and H. Hashemi, "True-time-delay-based multi-beam arrays," *IEEE Trans. Microw. Theory Techn.*, vol. 61, no. 8, pp. 3072–3082, Aug. 2013.

[7] O. Raz, S. Barzilay, R. Rotman, and M. Tur, "Submicrosecond scan-angle switching photonic beamformer with flat RF response in the C and X bands," *J. Lightw. Technol.*, vol. 26, no. 15, pp. 2774–2781, Aug. 1, 2008.

[8] L. Yaron, R. Rotman, S. Zach, and M. Tur, "Photonic beamformer receiver with multiple beam capabilities," *IEEE Photon. Technol. Lett.*, vol. 22, no. 23, pp. 1723–1725, Dec. 15, 2010.

[9] B. Zhou, X. Zheng, X. Yu, H. Zhang, Y. Guo, and B. Zhou, "Optical beamforming networks based on broadband optical source and chirped fiber grating," *IEEE Photon. Technol. Lett.*, vol. 20, no. 9, pp. 733–735, May 1, 2008.

[10] X. Xue, H. Wen, X. Zheng, H. Zhang, Y. Guo, and B. Zhou, "Noise analysis in photonic true time delay systems based on broadband optical source and dispersion components," *Appl. Opt.*, vol. 48, no. 4, pp. 658–663, Feb. 2009.

[11] J. D. Shin, B. S. Lee, and B. G. Kim, "Optical true time-delay feeder for X-band phased array antennas composed of 2×2 optical MEMS switches and fiber delay lines," *IEEE Photon. Technol. Lett.*, vol. 16, no. 5, pp. 1364–1366, May 2004.

[12] R. Chen, X. Zheng, and H. Zhang, "The error of optical true time delay network caused by optical switches," in *Proc. SPIE*, vol. 5625, Feb. 2005, pp. 519–527.

[13] A. Yu, W. Zou, S. Li, and J. Chen, "A multi-channel multi-bit programmable photonic beamformer based on cascaded DWDM," *IEEE Photon. J.*, vol. 6, no. 4, pp. 1–10, Aug. 2014.

[14] C. Fan, S. Huang, X. Gao, J. Zhou, W. Gu, and H. Zhang, "Compact high frequency true-time-delay beamformer using bidirectional reflectance of the fiber gratings," *Opt. Fiber Technol.*, vol. 19, no. 1, pp. 60–65, Jan. 2013.

[15] Y. Liu, J. Yang, and J. Yao, "Continuous true-time-delay beamforming for phased array antenna using a tunable chirped fiber grating delay line," *IEEE Photon. Technol. Lett.*, vol. 14, no. 8, pp. 1172–1174, Aug. 2002.

[16] B. Ortega, J. L. Cruz, J. Capmany, M. V. Andres, and D. Pastor, "Variable delay line for phased-array antenna based on a chirped fiber grating," *IEEE Trans. Microw. Theory Techn.*, vol. 48, no. 8, pp. 1352–1360, Aug. 2000.

[17] Y. Jiang et al., "Dispersion-enhanced photonic crystal fiber array for a true time-delay structured X-band phased array antenna," *IEEE Photon. Technol. Lett.*, vol. 17, no. 1, pp. 187–189, Jan. 1, 2005.

[18] H. Subbaraman, M. Y. Chen, and R. T. Chen, "Photonic crystal fiber-based true-time-delay beamformer for multiple RF beam transmission and reception of an X-band phased-array antenna," *J. Lightw. Technol.*, vol. 26, no. 15, pp. 2803–2809, Aug. 1, 2008.

[19] P. Wu, S. Tang, and D. E. Raible, "A prototype high-speed optically-steered X-band phased array antenna," *Opt. Exp.*, vol. 21, no. 26, pp. 32599–32604, Dec. 2013.

[20] J. L. Corral, J. Marti, J. M. Fuster, and R. I. Laming, "True time-delay scheme for feeding optically controlled phased-array antennas using chirped-fiber gratings," *IEEE Photon. Technol. Lett.*, vol. 9, no. 11, pp. 1529–1531, Nov. 1997.

[21] T. Mengual et al., "Optical phase-based beamformer using MZM SSB modulation combined with crystal polarization optics and a spatial light modulator," *Opt. Commun.*, vol. 281, no. 2, pp. 217–224, Jan. 2008.

[22] B. Vidal, T. Mengual, and J. Martí, "Fast optical beamforming architectures for satellite-based applications," *Adv. Opt. Technol.*, vol. 2012, pp. 1–5, Oct. 2012.

[23] T. Nagayama, S. Akiba, T. Tomura, and J. Hirokawa, "Photonics-based millimeter-wave band remote beamforming of array-antenna integrated with photodiode using variable optical delay line and attenuator," *IEEE/OSA J. Lightw. Technol.*, vol. 36, no. 19, pp. 4416–4422, Oct. 1, 2018.

[24] H. Zmuda, R. A. Soref, P. Payson, S. Johns, and E. N. Toughlian, "Photonic beamformer for phased array antennas using a fiber grating prism," *IEEE Photon. Technol. Lett.*, vol. 9, no. 2, pp. 241–243, Feb. 1997.

[25] M. L. Lees, "Digital beamforming calibration for FMCW radar," *IEEE Trans. Aerosp. Electron. Syst.*, vol. AES-25, no. 2, pp. 281–284, Mar. 1989.

[26] D. B. Hunter, M. E. Parker, and J. L. Dexter, "Demonstration of a continuously variable true-time delay beamformer using a multichannel chirped fiber grating," *IEEE Trans. Microw. Theory Techn.*, vol. 54, no. 2, pp. 861–867, Feb. 2006.

[27] H. Matsuzaw et al., "Variable spot scanning antenna using optically controlled beam forming network," in *Proc. Int. Top. Meet. Microw. Photon. Conf.*, Oct. 2010, pp. 397–400.

[28] K.-H. Lee, Y. M. Jhon, and W.-Y. Choi, "Photonic phase shifters based on a vector-sum technique with polarization-maintaining fibers," *Opt. Lett.*, vol. 30, no. 7, p. 702, Apr. 2005.

[29] L. A. Bui, A. Mitchell, K. Ghorbani, T. H. Chio, S. Mansoori, and E. R. Lopez, "Multichannel vector sum phase shifter," *Opt. Lett.*, vol. 31, no. 5, pp. 577–579, Mar. 2006.

[30] L. Yan et al., "Programmable group-delay module using binary polarization switching," *IEEE/OSA J. Lightw. Technol.*, vol. 21, no. 7, pp. 1676–1684, Jul. 1, 2003.

[31] S. Li, T. Qing, J. Fu, X. Wang, and S. Pan, "High-accuracy optical fiber transfer delay measurement using fiber-optic microwave interferometry," *J. Lightw. Technol.*, vol. 39, no. 2, pp. 627–632, Jan. 15, 2021.

[32] X. Ye, D. Zhu, Y. Zhang, S. Li, and S. Pan, "Analysis of photonics-based RF beamforming with large instantaneous bandwidth," *J. Lightw. Technol.*, vol. 35, no. 23, pp. 5010–5019, Dec. 1, 2017.

[33] X. Ye, B. Zhang, Y. Zhang, D. Zhu, and S. Pan, "Performance evaluation of optical beamforming-based wideband antenna array," *Chin. Opt. Lett.*, vol. 15, no. 1, Jan. 2017, Art. no. 010013.